




Cite this: *RSC Adv.*, 2017, 7, 36935

# Upconversion luminescence enhancement and temperature sensing behavior of F<sup>-</sup> co-doped Ba<sub>3</sub>Lu<sub>4</sub>O<sub>9</sub>:Er<sup>3+</sup>/Yb<sup>3+</sup> phosphors†

Songbin Liu,<sup>a</sup> Shuifu Liu,<sup>a</sup> Ming Zhou,<sup>a</sup> Xinyu Ye,<sup>b</sup> \*<sup>ab</sup> Dejian Hou<sup>a</sup> and Weixiong You<sup>c</sup>

A series of Ba<sub>3</sub>Lu<sub>4</sub>O<sub>9</sub>:Er<sup>3+</sup>/Yb<sup>3+</sup> (EYBLO) phosphors co-doped with F<sup>-</sup> ions were synthesized by a simple solid-state reaction method. The results showed that the primary rhombohedral structure was maintained and the crystal lattice began to shrink when F<sup>-</sup> ions were introduced into the host matrix to occupy the O<sup>2-</sup> site. The agglomerations and the impurities (OH<sup>-</sup> and CO<sub>2</sub>) with higher phonon energy on the sample surface could be minimized and the sample crystallinity could be improved. Under 980 nm laser diode excitation, the green and red UC emissions of the EYBLO:0.4F<sup>-</sup> sample show nearly 5- and 7.5-fold enhancements in contrast to F<sup>-</sup>-free EYBLO. The upconversion luminescence can be finely tuned from yellow to red light to some extent by increasing F<sup>-</sup> concentration. Based on pump-power dependence and decay lifetime analysis, the energy level diagram was illustrated and the upconversion energy-transfer mechanism was discussed. The green and red emission enhancements are attributed to the modification of the local crystal field of Er<sup>3+</sup> ions and reduction of crystal site symmetry. The cross-relaxation and back-energy-transfer processes play an important role to enhance the red/green UC emission intensity ratios. The fluorescence intensity ratio technique was employed to investigate the temperature sensing behavior of the synthesized phosphors. The temperature sensing properties can be enhanced by doping of F<sup>-</sup> ions, and the maximum sensitivity is found to be 44.57 × 10<sup>-4</sup> K<sup>-1</sup> at 523 K. It is promising to provide an alternative approach for enhancing UC luminescence and the temperature sensitivity in oxide matrixes and then obtain high-quality optical temperature-sensing materials by simply co-doping F<sup>-</sup> ions.

Received 31st May 2017  
 Accepted 21st July 2017

DOI: 10.1039/c7ra06054h

[rsc.li/rsc-advances](http://rsc.li/rsc-advances)

## 1. Introduction

Upconversion (UC) is a typically anti-Stokes emission process, which can convert long-wavelength excitation into short-wavelength light output by means of energy transfer and excited state absorption. Over the past decade, UC luminescence has attracted great attention in diverse research fields.<sup>1,2</sup> In particular, rare earth (RE) ion-doped UC luminescence materials are one of the research hotspots in this area for their potential applications in biological imaging, compact solid state lasers, optical temperature sensors and solar energy conversion, *etc.*<sup>3,4</sup> Owing to their abundant ladder-like energy levels and relatively long excited-state lifetimes, trivalent RE ions such as Er<sup>3+</sup>, Tm<sup>3+</sup> or Ho<sup>3+</sup> are usually selected as

activators.<sup>5</sup> However, one of the drawbacks of the above RE<sup>3+</sup> ions is that they have low absorption cross-sections for 4f–4f transitions, which result in the low luminescence intensity for these transitions.<sup>6</sup> Yb<sup>3+</sup> ions are commonly used as sensitizers in UC luminescence materials due to their relatively large absorption cross-section at 980 nm, leading to efficient absorption of infrared (IR) or near-infrared (NIR) pump photons and subsequently transfer their harvest energy to neighboring activator ions.<sup>7</sup> Although there exists an effective energy-transfer (ET) from Yb<sup>3+</sup> to Er<sup>3+</sup>/Tm<sup>3+</sup>/Ho<sup>3+</sup>, the UC luminescence intensity of this type of material is still inadequate, which greatly limits their applications. Therefore, enhancing the UC luminescence intensity is one of the significant issues and great challenge for its actual application.

Recently, many kinds of techniques were adopted to improve the UC emission intensity, such as changing the crystal phase of host materials,<sup>8,9</sup> adding Nb to reduce phonon energy,<sup>10</sup> incorporating impurities such as Li<sup>+</sup>, Zn<sup>2+</sup> to modify the local crystal field around RE<sup>3+</sup> ions,<sup>11–13</sup> introducing core-shell structure,<sup>14</sup> and crystal surface coating.<sup>15</sup> It is well-known that the UC emission intensity of RE<sup>3+</sup> doped phosphor is strongly dependent on their intra 4f–4f transition possibility.<sup>16</sup> Therefore, UC emission intensity also could be enhanced by inhibiting non-

<sup>a</sup>School of Metallurgy and Chemistry Engineering, Jiangxi University of Science and Technology, Ganzhou 341000, P. R. China. E-mail: xinyue@yahoo.com

<sup>b</sup>National Engineering Research Center for Ionic Rare Earth, Ganzhou 341000, P. R. China

<sup>c</sup>School of Material Science and Engineering, Jiangxi University of Science and Technology, Ganzhou 341000, P. R. China

† Electronic supplementary information (ESI) available. See DOI: 10.1039/c7ra06054h



radiative (NR) transition process by means of using a host material with low phonon energy, such as fluoride and sulfide matrixes.<sup>17</sup> According to the energy-gap law, it is especially important for the UC luminescence processes are very sensitive to quenching by high-energy vibration.<sup>18</sup> Moreover, F<sup>-</sup> ions can be doped into the matrices efficiently by substitution of O<sup>2-</sup> sites in the crystal lattice due to their similar electronic configuration and nearly same ionic radius.<sup>19,20</sup> In down-conversion system, the influence of fluoride on f-f transition of Eu<sup>3+</sup> was investigated, and the results showed that substitution of F<sup>-</sup> for O<sup>2-</sup> might reduce the magnitude of the phonon energy and quenched NR transition processes to enhance the luminescence intensity.<sup>21,22</sup> In addition, Sun *et al.* reported that the replacement of OH<sup>-</sup> by F<sup>-</sup> can improve the luminescence intensity significantly, which may be caused by the decreased fluorescence quenching of activator ion.<sup>23</sup> Compared with down-conversion system,<sup>21,22</sup> there exist very few reports about the enhancement of luminescence by co-doped F<sup>-</sup> ions in upconversion luminescence material. Recently, Li *et al.*<sup>24</sup> reported an efficient F<sup>-</sup> anion doping strategy to enhance upconversion luminescence in NaGd(MoO<sub>4</sub>)<sub>2</sub>:Yb<sup>3+</sup>/Er<sup>3+</sup> nanophosphors, based on the Rietveld refinements and Judd-Ofelt analysis. The luminescence enhancement is due to the fact that the doping of F<sup>-</sup> augmented local crystal field strength, lowered site symmetry, and inhibited non-radiative transition of lanthanide activators.<sup>24</sup>

In various actual applications of UC luminescence, fluorescence-based optical temperature sensors have attracted much attention due to their peculiar characteristics: lower signal-to-noise ratio (SNR) and suitable for hazardous environments where are not possible for conventional thermocouple temperature detectors in oil refineries, coal mines and corrosive conditions.<sup>25,26</sup> Among these applications, the temperature-dependent fluorescence lifetime and fluorescence intensity ratio (FIR) are regarded as very promising techniques for optical temperature sensors. The FIR technique based on the measurement of luminescence intensities from two thermally coupled levels of RE<sup>3+</sup> ions is independent of signal losses and fluctuation in the excitation intensity and has the potential to improve measurement accuracy and resolution significantly.<sup>27,28</sup> In addition, the Er<sup>3+</sup> ions have been investigated extensively due to its green UC emissions originating from two thermally coupled levels <sup>2</sup>H<sub>11/2</sub> and <sup>4</sup>S<sub>3/2</sub>.<sup>29</sup> Therefore, it is meaningful for searching for a new Er<sup>3+</sup>-doped host materials and providing a practical method to enhance the sensitivity for high-quality optical temperature sensors. Moreover, no temperature sensing studies have been conducted on Er<sup>3+</sup>/Yb<sup>3+</sup> co-doped and F<sup>-</sup> tri-doped Ba<sub>3</sub>Lu<sub>4</sub>O<sub>9</sub> phosphor.

In our previous study, complex oxide-Ba<sub>3</sub>Lu<sub>4</sub>O<sub>9</sub> was found to be a promising upconversion phosphor host. Er<sup>3+</sup>/Yb<sup>3+</sup> co-doped Ba<sub>3</sub>Lu<sub>4</sub>O<sub>9</sub> phosphors exhibited intense and color-tunable UC luminescence under the 980 nm laser diode (LD) excitation.<sup>30</sup> The optimal Er<sup>3+</sup>/Yb<sup>3+</sup> doping concentration and sintering temperature were confirmed to be Ba<sub>3</sub>Lu<sub>3.3</sub>Er<sub>0.1</sub>Yb<sub>0.6</sub>O<sub>9</sub> at 1550 °C.<sup>30</sup> Herein, we report an enhancement of UC luminescence and temperature sensing behavior of Ba<sub>3</sub>Lu<sub>4</sub>O<sub>9</sub>:Er<sup>3+</sup>/Yb<sup>3+</sup> (EYBLO) phosphor by incorporation of F<sup>-</sup> ions. This

research focuses on the influences of F<sup>-</sup> ions doping on structure, morphology, UC luminescence and temperature sensing behavior. In combination with pump-power dependence, decay lifetime and energy level diagram, the improvement mechanisms of UC emission intensity by introducing F<sup>-</sup> ions into EYBLO are investigated in detail. The FIR technique is employed to study the temperature sensing behavior.

## 2. Experimental section

### 2.1 Preparation

The Ba<sub>3</sub>Lu<sub>4-y-z</sub>Er<sub>y</sub>Yb<sub>z</sub>O<sub>9-x/2</sub>F<sub>x</sub> (x = 0, 0.1, 0.2, 0.3, 0.4, 0.5, 0.6, y = 0.1 and z = 0.6) samples were prepared through a high-temperature solid-state reaction method. BaCO<sub>3</sub> (A.R.), Lu<sub>2</sub>O<sub>3</sub> (99.99%), Er<sub>2</sub>O<sub>3</sub> (99.99%) and Yb<sub>2</sub>O<sub>3</sub> (99.99%) were used as starting materials. For the purpose of without introducing impurity element, BaF<sub>2</sub> was selected as fluorine source; BaF<sub>2</sub> and BaCO<sub>3</sub> were used as barium source at the same time. According to certain stoichiometric ratio, the chemicals were weighed accurately and ground thoroughly in an agate mortar with some alcohol. Then the mixture was dried in an oven under the temperature of 60 °C for 15 min. The dried mixture powders were reground for 45 min and transferred into alumina crucibles. The sintering is performed at a rate of 5 °C per min to the specific temperatures (1200–1650 °C) and kept for 6 h in air. After sintering, the powders were furnace-cooled naturally down to room temperature. Finally, the as-prepared powders were washed with deionized water three times and dried at 120 °C for 3 h in a drying box to obtain final phosphors.

### 2.2 Characterization

The X-ray diffraction (XRD) measurements were performed by using a PANalytical X'Pert Pro diffractometer (Holland) with Cu K<sub>α1</sub> radiation (λ = 0.1540598 nm) operating at 40 kV and 40 mA to identify the structure and phase purity. All the XRD data within the range from 10° to 80° were recorded in a continuous scanning type with a scan step size of 0.01313°. The Fourier-transform infrared (FT-IR) spectra were obtained in the transmission mode on a Bruker (Karlsruhe, Germany) spectrophotometer in the range of 400–4000 cm<sup>-1</sup>. The samples were mixed with the potassium bromide (KBr) in 1 : 100 mass ratio to get a transparent pellet. The X-ray photoelectron spectroscopy (XPS) was carried out on the Escalab 250Xi (Thermo scientific, America) system using a monochromatic AlK<sub>α</sub> (hν = 1486.6 eV) X-ray source operating at 15 kV. The spectra were obtained at ambient temperature with an ultrahigh vacuum. The binding energies were charge-corrected using the C 1s peak of graphite at 284.6 eV as a reference. The morphologies of the samples were analyzed by field-emission scanning electron microscope (FE-SEM, TESCAN MIRA3 LMH, Czech Republic) equipped with the energy dispersive spectrum (EDS). The UC emission spectra in the wavelength range of 500–750 nm was collected by using a FluoroLog-3 (HORIBA Jobin Yvon, France) spectrophotometer equipped with an NIR Photomultiplier (R928, Hamamatsu, Japan). An external power-controllable 980 nm semiconductor laser diode was selected as excitation pump source. In order to



investigate the temperature dependence of the UC emission, the samples were placed in a temperature-controlled copper cylinder, and test temperature was increased from 293 to 573 K. The luminescence decay curves and NIR luminescence spectra were measured with a FLS980 (Edinburgh, England) spectrometer upon selective 980 nm excitation provided by an optical parametric oscillator (OPO). All the measurements were conducted at room temperature except for the temperature dependence of UC luminescence spectra test.

### 3. Results and discussion

#### 3.1 Structure and morphology

The  $\text{Ba}_3\text{Lu}_4\text{O}_9$  (BLO) crystal belongs to a rhombohedral structure with space group  $R\bar{3}$  (no. 146),<sup>31</sup> and cell parameters of  $a = b = 0.603$  nm,  $c = 2.4753$  nm. The XRD patterns of  $\text{F}^-$  ions co-doped  $\text{Ba}_3\text{Lu}_4\text{O}_9:\text{Er}^{3+}/\text{Yb}^{3+}$  (EYBLO) prepared at various

temperatures are shown in Fig. 1(a). All patterns of the samples sintered below 1550 °C match well with the standard reference of  $\text{Ba}_3\text{Lu}_4\text{O}_9$  (JCPDS No. 01-077-0323) and no impurity diffraction peaks are observed. However, when the temperature exceeds 1550 °C, the second phase  $\text{Lu}_2\text{O}_3$  begins to appear. Meanwhile, the diffraction peaks become markedly weaker instead of sharper and stronger from 1200 °C to 1500 °C. In addition, an interesting phenomenon is observed in the figure. The strongest diffraction peak belongs to (110) crystal plane when the sintering temperature below 1550 °C and then shifts to the (107) crystal plane as the temperature rising. It may be due to the preferred orientation of crystal growth along different direction at various sintering temperatures.<sup>32</sup>

Fig. 1(b) shows the XRD patterns of EYBLO co-doped with various  $\text{F}^-$  ( $x = 0-0.6$ ) ions. Within the range of experimental dopant concentration, all the observed diffraction peaks of  $\text{F}^-$  co-doped samples are exactly assigned to the pure phase

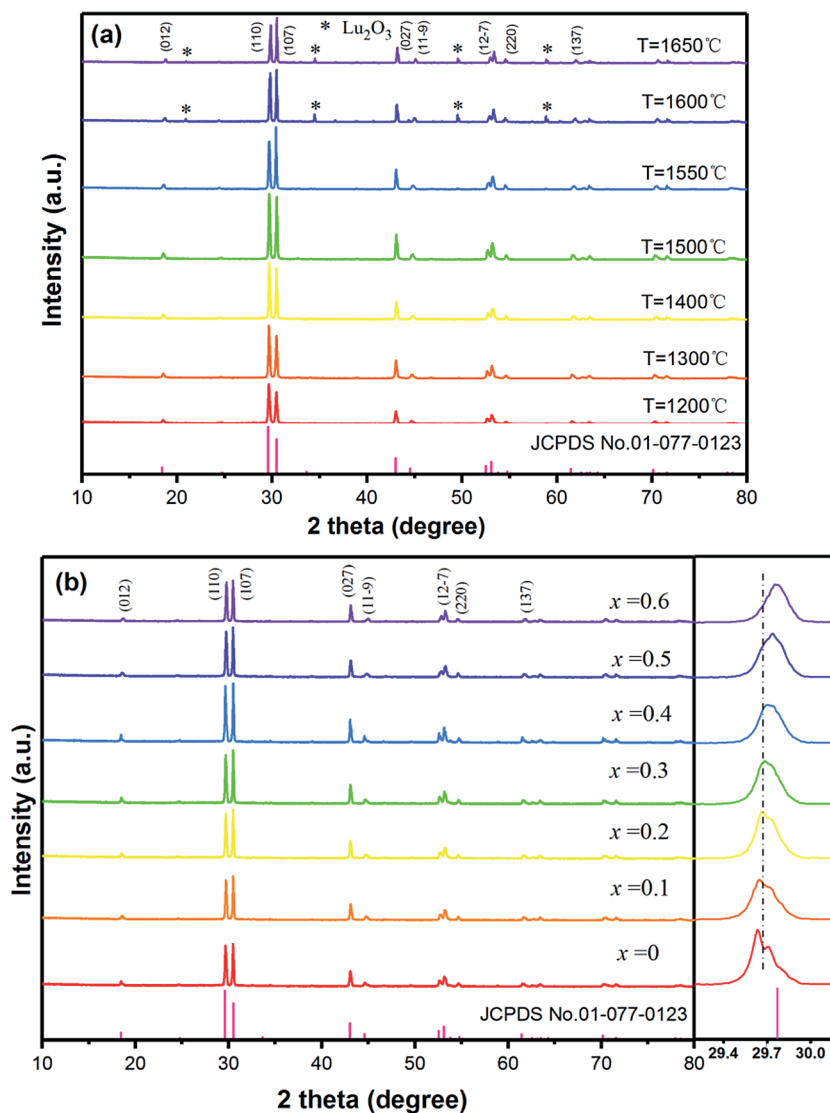


Fig. 1 (a) XRD patterns of EYBLO: $x\text{F}^-$  sample ( $x = 0.4$ ) at different sintering temperatures from 1200 °C to 1650 °C; (b) XRD patterns and magnified XRD patterns around (110) peak of EYBLO: $x\text{F}^-$  samples ( $x = 0-0.6$ ). The standard data for  $\text{Ba}_3\text{Lu}_4\text{O}_9$  (JCPDS No. 01-077-0123) is also presented in the figure.



$\text{Ba}_3\text{Lu}_4\text{O}_9$ . The results imply that  $\text{Er}^{3+}/\text{Yb}^{3+}/\text{F}^-$  tri-doped do not change the crystal structure of the host lattice. Comparing with the  $\text{F}^-$ -free sample ( $x = 0$ ), the intensities of diffraction peaks increase with increasing  $\text{F}^-$  ions doping concentration, which indicates that sample crystallinity can be enhanced by incorporation of  $\text{F}^-$  ions. When the doping concentration exceeds  $x = 0.4$ , the intensity of diffraction peaks decrease, which maybe result from the creation of surface defect by doping excessive  $\text{F}^-$  ions. Meanwhile, the magnified patterns around the (110) diffraction peak of  $\text{F}^-$  ions co-doped samples from  $2\theta = 29.2$ – $30.2^\circ$  is presented in the figure. Due to the same ionic valence state and similar ionic radius, the  $\text{Lu}^{3+}$  ions are substituted easily by  $\text{Yb}^{3+}/\text{Er}^{3+}$  ions.<sup>30</sup> It is obviously observed that the peak position corresponding to (110) slightly shifts towards the higher  $2\theta$  side with increasing  $\text{F}^-$  ions concentration. The phenomenon can be ascribed that smaller radii of  $\text{F}^-$  (0.133 nm, CN = 6) ions enter into the crystal lattice by occupying larger radius of  $\text{O}^{2-}$  (0.140 nm, CN = 6) ions.<sup>18</sup> It also indicates the successful doping of  $\text{F}^-$  ions in the EYBLO lattice.

To investigate the chemical compositions of the  $\text{F}^-$ -doped EYBLO samples, the XPS measurement was performed. All XPS data of elements were charge-corrected with respect to C 1s ( $\approx 284.6$  eV). The survey scan of core binding energy (BE) of

EYBLO: $x\text{F}^-$  ( $x = 0.4$ ) sample is presented in Fig. 2(a). The XPS peaks show that the  $\text{F}^-$ -doped EYBLO samples contain only Ba, Lu, O, Er, Yb and F and a trace amount of C. The C element is ascribed to the adventitious carbon from the XPS instrument itself. The inset is the magnified XPS spectrum to show the existence of Er 4d and Yb 4d. For the  $\text{F}^-$ -free EYBLO sample, the high-resolution XPS spectrum of Ba 3d spectrum exhibits two peaks,  $3d_{5/2}$  and  $3d_{3/2}$  (from the spin-orbit splitting),<sup>33</sup> located at 779.6 eV and 795.0 eV, respectively (ESI, Fig. S1(a)†). With increasing  $\text{F}^-$  doping concentration, no shifts are observed in the peak positions of  $3d_{5/2}$  and  $3d_{3/2}$ . Similarly, no move is found for the two peaks corresponding to Lu 4d, which have core BEs of  $\sim 196.2$  eV ( $3d_{5/2}$ ) and 206.0 eV ( $3d_{3/2}$ ),<sup>34</sup> after  $\text{F}^-$  ions incorporation (ESI, Fig. S1(b)†). These results confirm that the valence state of Ba and Lu elements maintain with the doping of  $\text{F}^-$  ions. In addition, because of the lower doping concentrations of  $\text{Er}^{3+}$  and  $\text{Yb}^{3+}$ , a comparatively low intensity was observed (ESI, Fig. S1(c and d)†). However, the F element is not detectable in the XPS spectrum (Fig. 3(b)) because of the low molar percent of F (about 0.1%). Meanwhile, the volatilization characteristics and light atomic mass of F bring some difficulties in detecting  $\text{F}^-$  ions. Therefore, the XPS spectrum of O 1s are used as a probe to find out the evident of the substitution of

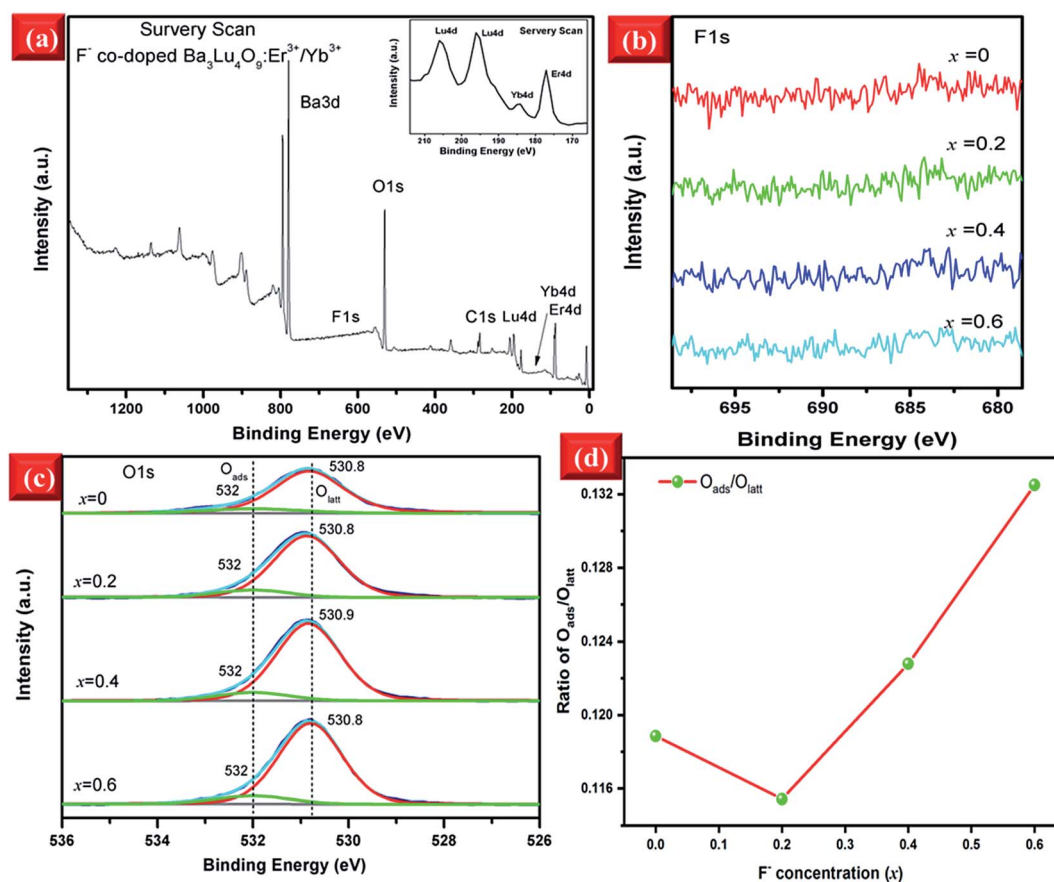


Fig. 2 (a) The survey scan XPS spectrum of EYBLO: $x\text{F}^-$  sample ( $x = 0.4$ ), the inset is the magnified XPS spectrum to show the existence of Er 4d and Yb 4d; (b) XPS spectra of F1s of EYBLO: $x\text{F}^-$  sample ( $x = 0, 0.2, 0.4$  and  $0.6$ ); (c) two deconvoluted peaks of O 1s, one located at  $\sim 532$  eV derives from the surface adsorption oxygen ( $\text{O}_{\text{ads}}$ ), and the other centered at  $\sim 530.8$  eV originates from the surface lattice oxygen ( $\text{O}_{\text{latt}}$ ) which can be substituted by  $\text{F}^-$  ions; (d) the integrated peak area ratios of  $\text{O}_{\text{ads}}$  and  $\text{O}_{\text{latt}}$  as a function of  $\text{F}^-$  dopant concentration.





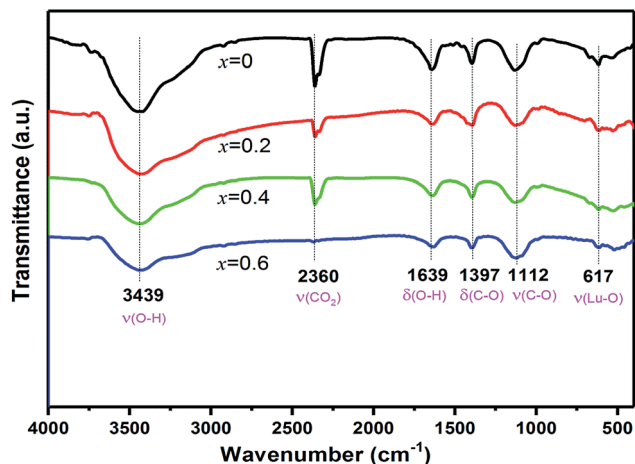


Fig. 3 FT-IR spectra of EYBLO: $x\text{F}^-$  samples ( $x = 0, 0.2, 0.4$  and  $0.6$ ) sintered at  $1500\text{ }^\circ\text{C}$ .

$\text{F}^-$  for  $\text{O}^{2-}$  and the changes of chemical surrounding environment of oxygen element.

Two deconvoluted peaks of O 1s regions are shown in Fig. 2(c). In the case of  $\text{F}^-$ -free EYBLO sample, the main contribution peak located at  $\sim 530.8\text{ eV}$  with FWHM  $\sim 1.56\text{ eV}$  is from the surface lattice oxygen ( $\text{O}_{\text{latt}}$ ), which could be substituted by  $\text{F}^-$  ions on the surface.<sup>35</sup> And the weak contribution peak centered at  $\sim 532\text{ eV}$  with FWHM  $\sim 1.83\text{ eV}$  is from the surface adsorption oxygen ( $\text{O}_{\text{ads}}$ ) physically adsorbed on the surface.<sup>36</sup> With increasing  $\text{F}^-$  co-doping concentrations, the two peak positions and FWHM have slightly shifts of about  $0.1\text{ eV}$  and  $0.68\text{ eV}$ , respectively. The BE of O 1s increases with increasing  $\text{F}^-$  ion doping content. The shift of the BE of the  $\text{O}_{\text{latt}}$  to the higher value could be interpreted as an increase of electronegativity ( $\text{F}^- > \text{O}^{2-}$ ) on the surface because of the effective substitution of  $\text{F}^-$  for  $\text{O}^{2-}$ . Therefore, increasing of basic strength of the oxygen atoms results in the enhancement of the bond energy.<sup>37</sup> So the variation tendency of O 1s BE can provide an evident that the  $\text{O}^{2-}$  can be substituted successfully by  $\text{F}^-$  ions. Meanwhile, the intensities of O 1s peaks keep declining monotonically with the increase of  $\text{F}^-$  concentration, which can also explain indirectly that reduction of oxygen content is due to the effective substitution by  $\text{F}^-$  ions. Further, the ratio of integrated peak areas of  $\text{O}_{\text{ads}}$  and  $\text{O}_{\text{latt}}$  as a function of  $\text{F}^-$  ions doped concentration are shown in Fig. 2(d). Compared with the  $\text{F}^-$ -free doped sample, the ratio of  $\text{O}_{\text{ads}}/\text{O}_{\text{latt}}$  of  $\text{F}^-$  doped EYBLO: $x\text{F}^-$  ( $x = 0.2$ ) is lower, which probably caused by the creation of oxygen ion vacancies and/or surface defects through the sample surface with the introduction of  $\text{F}^-$  ions into the host matrix.<sup>26,38</sup> Nevertheless, it begins to increase when the  $\text{F}^-$  ions doping concentration exceeds  $x = 0.2$ . The substitution of  $\text{F}^-$  for  $\text{O}^{2-}$  can result in the reduction of the amount of  $\text{O}_{\text{latt}}$  and enlargement of  $\text{O}_{\text{ads}}/\text{O}_{\text{latt}}$  ratio.

Fig. 3 shows the FT-IR spectra of EYBLO co-doped with various  $\text{F}^-$  ions ( $x = 0-0.6$ ). A broad peak at  $3439\text{ cm}^{-1}$  and a weak peak at  $1639\text{ cm}^{-1}$  originate from the stretching vibration and deformation of the  $\text{OH}^-$  group of water, respectively, which may be generated directly from the air.<sup>39</sup> Compared with

$\text{F}^-$ -free doped EYBLO sample, the absorption bands of  $\text{OH}^-$  group become weaker with adding  $\text{F}^-$  ions. Peak at  $2360\text{ cm}^{-1}$  is caused by the interference of  $\text{CO}_2$  in the air and the absorption nearly disappears by incorporation of  $\text{F}^-$  ions. The phonon energies of the  $\text{OH}^-$  group and  $\text{CO}_2$  are  $\sim 1500$  and  $\sim 3350\text{ cm}^{-1}$ , respectively. These higher energy phonon groups can be absorbed by the lattice surface to form the surface defects, which act as NR transition centers to quench the luminescence.<sup>40,41</sup> The relative absorption intensities of these groups are reduced by doping  $\text{F}^-$  into EYBLO samples, which indicates that higher phonon groups can be removed by incorporation of  $\text{F}^-$  ions. Therefore, it decreases the quenching centers and increases the UC luminescence intensities. The absorption peaks at  $1397\text{ cm}^{-1}$  and  $1112\text{ cm}^{-1}$  can be assigned to the asymmetric stretching vibration and stretching vibration of C-O bond, respectively. Whereas the peak at  $617\text{ cm}^{-1}$  is attributed to the characteristic stretching vibration of Lu-O bond.<sup>42</sup> Such absorption peaks have similar intensities for all  $\text{F}^-$ -doped and  $\text{F}^-$  free samples, which indicates that the interaction of Lu-O bond seldom changed with doping  $\text{F}^-$  ions.

The morphology of phosphor materials is an important factor for luminescence properties. The FE-SEM images of the EYBLO co-doped with various  $\text{F}^-$  ( $x = 0-0.6$ ) ions are shown in Fig. 4. It is observed that the morphologies and average particle size of samples have not been affected by different concentrations of  $\text{F}^-$  ions. Therefore, the luminescence enhancement of low content  $\text{F}^-$  doping is not due to the improvement of the sample morphology. Similar phenomenon can also observed in other literature by different cation or anion doping.<sup>24,43</sup> In addition, the EYBLO: $0.4\text{F}^-$  sample shows a narrow size distribution with average size of approximately  $2.7\text{ }\mu\text{m}$  (Fig. 4(f)). Moreover, Fig. 4(e) shows the EDS spectra of EYBLO: $0.4\text{F}^-$  sample. The actual chemical compositions contains Ba, Lu, Er, Yb, O, and F elements. Because the diffraction peaks of  $\text{BaF}_2$  phase are not shown in the XRD patterns, the existence of F element in the spectra suggests that  $\text{F}^-$  ions are successfully co-doped into the crystal structure.

In order to observe the distribution of the elements to confirm if the doped elements are uniformly dispersed in the host, the elemental mapping images of EYBLO: $0.4\text{F}^-$  sample were obtained by EDS measurement. Fig. 5(a) is the SEM image of the tested area, Fig. 5(b-f) exhibit the distributions of the different elements O, F, Lu, Er and Yb in the area, respectively. The EDS mapping results show that the F and O are uniformly distributed in the sample, which verifies that the  $\text{O}^{2-}$  site might be successfully occupied by the  $\text{F}^-$  via the high temperature solid-state reaction. In addition, the distributions of Lu, Er and Yb elements are homogeneous, and homogeneous distribution of activator ions in the host can reduce the concentration quenching and promote the luminescence intensity.<sup>44,45</sup>

### 3.2 Upconversion luminescence

Fig. 6 shows the UC emission spectra of EYBLO: $0.4\text{F}^-$  sample sintered at various temperatures from  $1200\text{ }^\circ\text{C}$  to  $1650\text{ }^\circ\text{C}$  under the excitation of  $980\text{ nm}$  LD. The inset of figure shows the emission intensity of green region ( $560\text{ nm}$ ) and red region



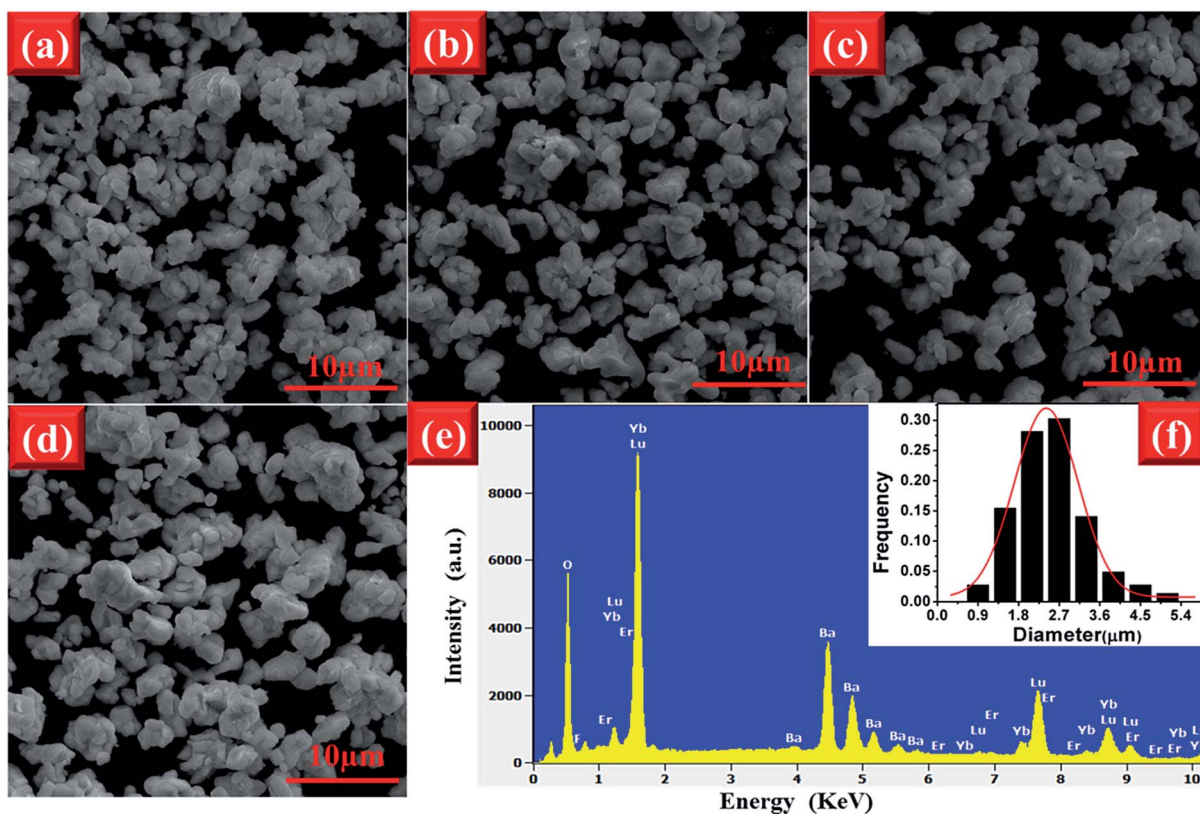


Fig. 4 FE-SEM images of EYBLO: $x\text{F}^-$  samples prepared at 1500 °C with (a)  $x = 0$ , (b)  $x = 0.2$ , (c)  $x = 0.4$ , (d)  $x = 0.6$ ; (e) the EDS spectrum and (f) the histogram of particle size distribution of EYBLO:0.4 $\text{F}^-$  samples sintered at 1500 °C.

(663 nm) as a function of sintering temperature. It is obvious that the green and red emission intensities enhance with sintering temperature increasing up to 1500 °C. When the temperature exceeds 1500 °C, the UC luminescence intensity decrease monotonously. It may be caused by the occurrence of impurity phase  $\text{Lu}_2\text{O}_3$  at higher sintering temperature.

In order to determine the optimal doping concentration of  $\text{F}^-$  ions, the dependence of the UC emission spectra on  $\text{F}^-$  doping contents were studied at room temperature under 980 nm LD excitation. The variation of UC emission intensities of EYBLO: $x\text{F}^-$  samples ( $x = 0-0.6$ ) are shown in Fig. 7. The UC spectra exhibit bright red emission with weak green emission. The intense red emission band centered at 663 nm is corresponding to the transition  $^4\text{F}_{9/2} \rightarrow ^4\text{I}_{15/2}$  of  $\text{Er}^{3+}$ . Two relatively weaker green emission bands centered at 537 nm and 560 nm can be attributed to the  $^2\text{H}_{11/2} \rightarrow ^4\text{I}_{15/2}$  and  $^4\text{S}_{3/2} \rightarrow ^4\text{I}_{15/2}$  electronic transitions of  $\text{Er}^{3+}$ , respectively. The spectra of all samples with different  $\text{F}^-$  concentrations are similar in shapes of emission bands and peak positions, but differ in luminescence intensity. The inset of the figure shows the digital photographs of EYBLO: $x\text{F}^-$  samples ( $x = 0$  and  $x = 0.4$ ) using a Nikon digital camera with suitable color filters. The luminescence color shifts from bright tallow ( $\text{F}^-$ -free doped EYBLO) to red light (EYBLO:0.4 $\text{F}^-$ ) to naked eye under 980 nm LD excitation. When the  $\text{F}^-$  doping concentrations varied from  $x = 0$  to  $x = 0.6$ , the UC emission color coordinates move from yellow region (0.5061, 0.4886) to red region (0.6228, 0.3743)

(ESI, Fig. S2<sup>†</sup>). Therefore, the UC emission color can be finely tuned from yellow to red light to some extent by adjusting  $\text{F}^-$  concentrations.

Fig. 8(a) shows the dependence of green emission (560 nm) and red emission (663 nm) intensities as well as Red/Green intensity ratio (R/G) on  $\text{F}^-$  concentrations. As we can see, the red and green emission intensities show the similar trends to  $\text{F}^-$  doping concentrations. Both emission intensities increase along with increasing  $\text{F}^-$  contents first, and then reach a maximum at  $x = 0.4$ . When the  $\text{F}^-$  concentration exceeds this threshold, the UC luminescence intensity decreases gradually. Compared with  $\text{F}^-$ -free sample, it is observed that the UC red emission intensity of EYBLO:0.4 $\text{F}^-$  sample is drastically increased by fold of 7.5, which is larger than 5 times enhancement for UC green emission. As demonstrated by the Raman spectra (ESI, Fig. S3<sup>†</sup>), the maximum phonon energy of  $\text{Ba}_3\text{Lu}_4\text{O}_9$  host matrix is almost identical to  $1205\text{ cm}^{-1}$  for all samples. The results indicate that the lattice vibration mode, and thereby multi-phonon relaxation rate, has not been altered by further introduction of different  $\text{F}^-$  ions. Therefore, the reduction of the phonon energy caused by  $\text{F}^-$  doping is inadequate to explain the enhancement of UC luminescence intensity. The enhancement reason may be attributed to at least the following three aspects. First and the most obvious one is the modification of the local crystal field around the  $\text{Er}^{3+}$  ions in the host lattice.<sup>24,43,46</sup> According to Laporte's parity selection rule, electric dipole  $4f-4f$  transitions of lanthanide ions are





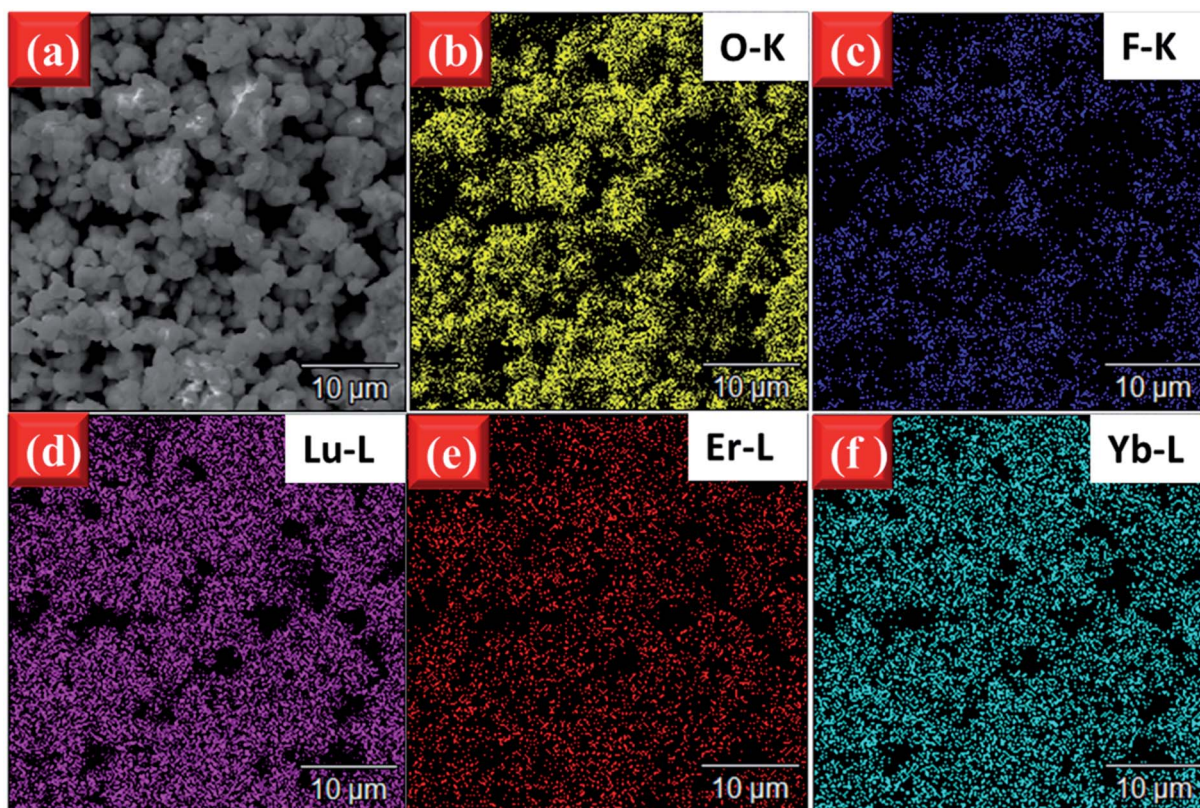


Fig. 5 (a) SEM image of tested area and EDS element mapping of (b) O–K, (c) F–K, (d) Lu–L, (e) Er–L, (f) Yb–L of EYBLO:0.4F<sup>−</sup> samples sintered at 1500 °C.

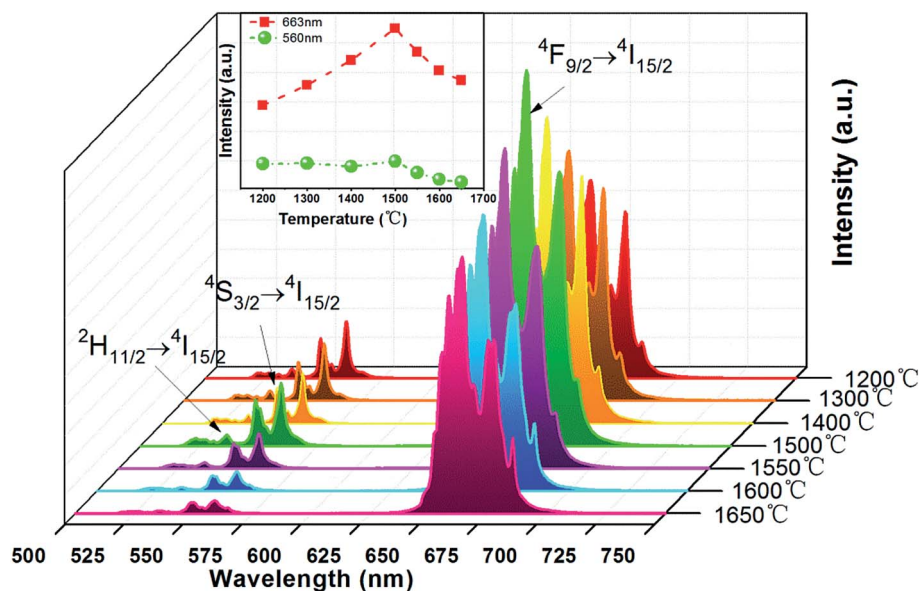


Fig. 6 UC emission spectra of EYBLO: $x$ F<sup>−</sup> samples ( $x = 0.4$ ) sintered at the temperatures from 1200 °C to 1650 °C under the excitation of 980 nm LD; the inset is green and red emission intensity as a function of sintering temperature.

forbidden due to the same parity of the 4f level. Just as discussed above, the incorporation of F<sup>−</sup> ions into the host matrix to occupy O<sup>2−</sup> site or enter interstitial sites would modify the local crystal field environment of Er<sup>3+</sup> ions, lower site symmetry

of the lanthanide activator ions and break the 4f–4f forbidden transitions to enhance the UC luminescence.<sup>16,26,39–41</sup> Secondly, the flux effect of BaF<sub>2</sub> could not be neglected and F<sup>−</sup> doping may also improve crystallinity and particle morphology of samples



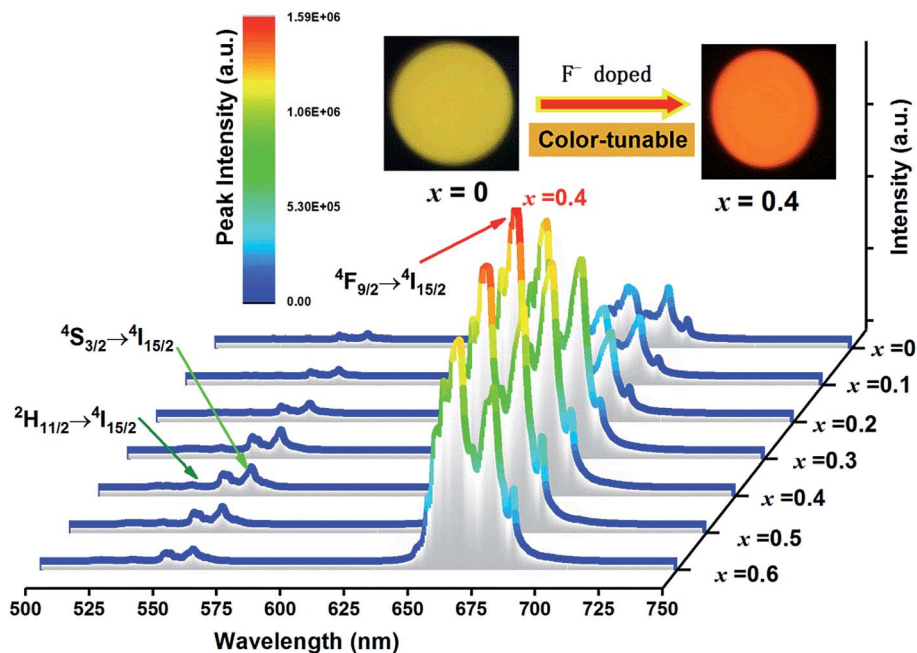


Fig. 7 UC emission spectra of EYBL0: $x\text{F}^-$  samples ( $x = 0-0.6$ ) under the excitation of 980 nm LD; the inset shows the digital photographs of EYBL0: $x\text{F}^-$  samples ( $x = 0$  and  $x = 0.4$ ) were recorded using a Nikon digital camera with a suitable color filters.

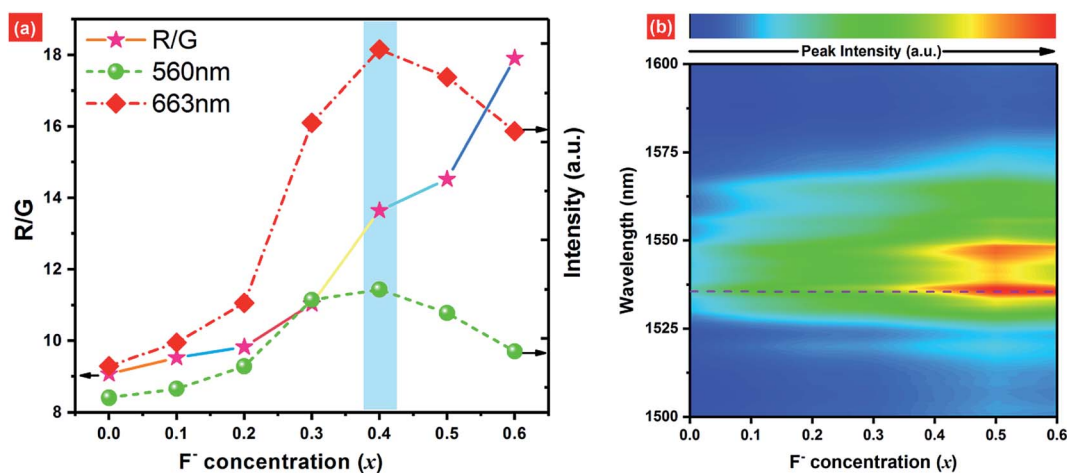


Fig. 8 (a) The UC green emission (560 nm) and red emission (663 nm) intensity as well as Red/Green ratio as a function of the  $\text{F}^-$  doped concentration; (b) the intensity map of the NIR emission spectra of EYBL0: $x\text{F}^-$  samples ( $x = 0-0.6$ ) within the range of 1500–1600 nm under the excitation of 980 nm LD.

as discussed in the Fig. 4, which further enhances the UC luminescence. In addition, higher phonon energy groups also can be reduced by incorporation by  $\text{F}^-$  ions, which contribute to the decrease of quenching center and increase of UC luminescence intensity. When continue to increase the  $\text{F}^-$  doping contents, the UC emission intensity decreases gradually, which means that the radiative transition probability become decrease. In other words, the non-radiative transition probability increases with increasing  $\text{F}^-$  content ( $x > 0.4$ ) due to the creation of sample surface defects induced excessive  $\text{F}^-$  ions.<sup>26</sup>

At the same time, the dependences of the emission intensity ratio of red and green (R/G) as a function of the  $\text{F}^-$  concentration

is presented in Fig. 8(a). The R/G keeps increasing monotonically from 9.069 to 17.907 with increasing  $\text{F}^-$  contents from  $x = 0$  to  $x = 0.6$ . The population of excited states  $^2\text{H}_{11/2}/^4\text{S}_{3/2}$  and  $^4\text{F}_{9/2}$  are all accomplished by NR transition from upper  $^4\text{F}_{7/2}$  level of  $\text{Er}^{3+}$  ions, then the electrons populated at above levels can relax radiatively to the ground state  $^4\text{I}_{15/2}$  to produce the green and red emission, respectively. The reason for R/G variation may be ascribed to the cross-relaxation (CR:  $^2\text{H}_{11/2}(\text{Er}^{3+}) + ^4\text{I}_{15/2}(\text{Er}^{3+}) \rightarrow ^4\text{I}_{9/2}(\text{Er}^{3+}) + ^4\text{I}_{13/2}(\text{Er}^{3+})$ ) between  $\text{Er}^{3+}$  ions or back-energy-transfer (BET:  $^4\text{S}_{3/2}(\text{Er}^{3+}) + ^2\text{F}_{7/2}(\text{Yb}^{3+}) \rightarrow ^4\text{I}_{13/2}(\text{Er}^{3+}) + ^2\text{F}_{5/2}(\text{Yb}^{3+})$ ) from  $\text{Er}^{3+}$  to  $\text{Yb}^{3+}$  ions to populate the  $^4\text{I}_{13/2}$  level of  $\text{Er}^{3+}$  ions.<sup>30,43,47,48</sup> Then the ET process,  $^4\text{I}_{13/2}(\text{Er}^{3+}) + ^2\text{F}_{5/2}(\text{Yb}^{3+}) \rightarrow ^4\text{F}_{9/2}$





(Er<sup>3+</sup>) + <sup>2</sup>F<sub>7/2</sub> (Yb<sup>3+</sup>), increases the population of the <sup>4</sup>F<sub>9/2</sub> level which eventually leads to produce more red emission and increase the R/G ratios. As we know, to substitute the O<sup>2-</sup> ions by smaller F<sup>-</sup> ions can induce the crystal lattice to shrink, leading to shorten the distances between adjacent Er<sup>3+</sup> and Er<sup>3+</sup> ions or and Yb<sup>3+</sup> ions.<sup>49</sup> Therefore, the rate of CR or BET processes can be accelerated with increasing F<sup>-</sup> doping concentration. Fig. 8(b) shows broad NIR luminescence spectra of EYBLO:xF<sup>-</sup> samples ( $x = 0-0.6$ ) within the range of 1500–1600 nm under 980 nm LD excitation. The dominant NIR emission centered at 1536 nm is assigned to the <sup>4</sup>I<sub>13/2</sub> → <sup>4</sup>I<sub>15/2</sub> transition of Er<sup>3+</sup>. The dependence of NIR emission on the F<sup>-</sup> doping concentrations is different with those of the red and green emission. The NIR emission intensities increase continuously with the increase of F<sup>-</sup> doping concentrations. It is well-known that the luminescence intensity is dependent on the number of the electrons populated in the upper excited state and the relative radiative transition probability.<sup>50</sup> These results strongly suggest that the number of the electrons populated in the <sup>4</sup>I<sub>13/2</sub> level can be accelerated by CR between Er<sup>3+</sup> ions or BET process from Er<sup>3+</sup> to Yb<sup>3+</sup> ions to accomplish population.

Fig. 9 presents the luminescence decay curves of 560 nm (<sup>4</sup>S<sub>3/2</sub> → <sup>4</sup>I<sub>15/2</sub>) and 663 nm (<sup>4</sup>F<sub>9/2</sub> → <sup>4</sup>I<sub>15/2</sub>) emissions of EYBLO:xF<sup>-</sup> samples with different F<sup>-</sup> doping concentrations under the excitation of 980 nm LD. Both the decay curves of green and red emissions show double exponential decay profiles, which fit well with second-order exponential decay mode, according to the following expression:<sup>51</sup>

$$I = A_1 \exp\left(-\frac{t}{\tau_1}\right) + A_2 \exp\left(-\frac{t}{\tau_2}\right) \quad (1)$$

where  $t$  is the time,  $I$  is the corresponding luminescence intensity at time  $t$ ,  $A_1$  and  $A_2$  are fitting constant,  $\tau_1$  and  $\tau_2$  are rapid and slow decay times for the exponential decay fitting, respectively. Moreover, the average lifetime  $\tau$  can be determined using the calculation below:<sup>51</sup>

$$\tau = \frac{A_1 \tau_1^2 + A_2 \tau_2^2}{A_1 \tau_1 + A_2 \tau_2} \quad (2)$$

The calculated average lifetime of Er<sup>3+</sup> are determined to be 79.735, 103.995, 111.418, 108.118  $\mu$ s and 81.679, 129.564, 167.580, 166.610  $\mu$ s for 560 nm and 663 nm emissions of the F<sup>-</sup> concentrations ( $x = 0, 0.2, 0.4$  and  $0.6$ ), respectively. It is evident that both the lifetime  $\tau$  of 560 nm and 663 nm emissions increase with the increase of F<sup>-</sup> doping concentration, then decrease slightly. This variation tendency is in accordance with changes of emission spectra in Fig. 7. Generally, the lifetime of an excited state depends on the probability of depopulation (radiative and non-radiative) transitions of electrons from this excited state.<sup>50</sup> The prolonged decay time of EYBLO:F<sup>-</sup> samples can be attributed to the modification of local crystal field of Er<sup>3+</sup> ions.<sup>28,45,51</sup> When appropriate F<sup>-</sup> ions were introduced into the host to occupy O<sup>2-</sup> sites, which given rise to the contraction of crystal lattice and hence lowered site symmetry. As more F<sup>-</sup> ions are introduced ( $x > 0.4$ ), the lifetime begins to decrease slightly. It may be correlative with the sample surface defects induced excessive F<sup>-</sup> ions, which can act as the non-radiative transition centers to quench the luminescence. Meanwhile, there exists a luminescence rise for 663 nm red emission (inset of Fig. 9(b)) compared with the green one. Therefore, a rise time manifests that additional ET process, rather than stepwise excited-state absorption (ESA) process to enhance the red emission. In addition, the lifetime of <sup>4</sup>I<sub>13/2</sub> level is about several milliseconds and increase with the increase of F<sup>-</sup> ions concentrations (ESI, Fig. S4<sup>†</sup>). The decay lifetime results can provide experiment evidence that the number of the electrons populated in the of <sup>4</sup>I<sub>13/2</sub> level can be accelerated by CR or BET process, leading to accelerate population of the <sup>4</sup>F<sub>9/2</sub> level *via* ET<sub>3</sub> process to produce more red emission. Therefore, this also coincides with the dependence of R/G on F<sup>-</sup> doping concentrations and explains why the R/G increases with increasing F<sup>-</sup> doping content.

### 3.3 Energy-transfer mechanism

In order to better understand the possible UC luminescence mechanism, the dependence of the UC emission intensity on the pump-power of 980 nm LD is investigated. The pump-power of LD was varied from 100–700 mW. With the increase of pump-

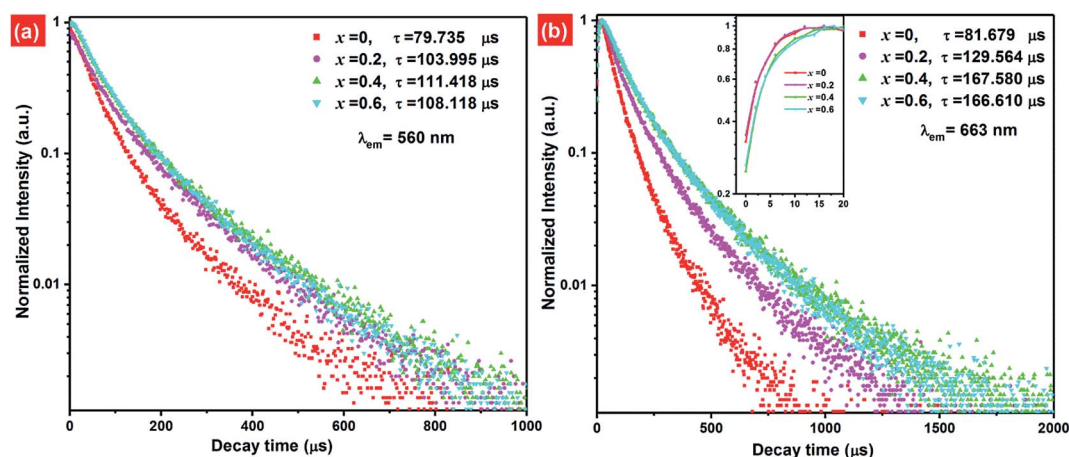


Fig. 9 Luminescence decay curves for EYBLO:xF<sup>-</sup> samples ( $x = 0, 0.2, 0.4$  and  $0.6$ ) at the (a) 560 nm (<sup>4</sup>S<sub>3/2</sub> → <sup>4</sup>I<sub>15/2</sub>) and (b) 663 nm (<sup>4</sup>F<sub>9/2</sub> → <sup>4</sup>I<sub>15/2</sub>) emissions under the excitation of 980 nm LD; the inset shows the luminescence rise curve.



power, the UC emission intensity increases remarkably, which indicates that the UC processes have not reached saturation at lower pump-power excitation (ESI, Fig. S5†). For the unsaturated upconversion process, at relatively lower pump-power excitation, the number of photons required to populate the upper emitting levels can be well described as follows:<sup>52</sup>

$$I_{\text{up}} \propto P_{\text{ex}}^n \quad (3)$$

where  $I_{\text{up}}$  is the UC emission intensity,  $P_{\text{ex}}$  is the pump-power of LD, and  $n$  is approximately equal to the number of pump photons required for UC process. The value  $n$  can be obtained from the slope of the straight line by linear fitting the plot of pump-power *versus* emission intensity in double logarithmic scales. As shown in Fig. 10(a), for the F<sup>-</sup>-free doped EYBLO sample, the slopes  $n$  for 537 nm emission ( ${}^2\text{H}_{11/2} \rightarrow {}^4\text{I}_{15/2}$ ), 560 nm emission ( ${}^4\text{S}_{3/2} \rightarrow {}^4\text{I}_{15/2}$ ) and 663 nm ( ${}^4\text{F}_{9/2} \rightarrow {}^4\text{I}_{15/2}$ ) are fitting to be 1.658, 1.741 and 1.981, respectively. Similarly, Fig. 10(b) shows the slopes  $n$  are 1.525, 1.619 and 1.861 for 537 nm, 560 nm and 663 nm emission in EYBLO:0.4F<sup>-</sup> sample, respectively, which are slightly smaller than the  $n$  value for the F<sup>-</sup>-free doped sample. These results confirm that two-photon absorption processes are involved in the observed green and red emissions in EYBLO samples both with and without F<sup>-</sup> ions. Because F<sup>-</sup> ions cannot absorb 980 nm pump photon energy, no energy transfer exists between Er<sup>3+</sup> and F<sup>-</sup> ions, which indicates that the mechanism of the UC luminescence to produce green and red emission was not changed by the incorporation of F<sup>-</sup> ions. Nevertheless, the  $n$  values alters slightly with F<sup>-</sup> ions and are smaller than that of F<sup>-</sup>-free doped EYBLO sample, which may be ascribed to the fact that the involved UC process occurs comparatively easily to saturate in F<sup>-</sup> co-doped than the F<sup>-</sup>-free EYBLO samples.<sup>16</sup>

Based on the pump-power dependence of UC emission intensity, the partial energy level diagram of Er<sup>3+</sup>/Yb<sup>3+</sup> and UC mechanism involved in green/red emission of F<sup>-</sup> co-doped

EYBLO phosphor under 980 nm excitation are presented in Fig. 11. Because of relatively large absorption cross-section of Yb<sup>3+</sup> ions around 980 nm, the ET process between Er<sup>3+</sup> and Yb<sup>3+</sup> plays a dominant role in the creation of UC luminescence. Firstly, the electrons at the ground state  ${}^2\text{F}_{7/2}$  of Yb<sup>3+</sup> ions are excited to  ${}^2\text{F}_{5/2}$  level by absorbing 980 nm pump photon energy, and then  ${}^4\text{I}_{11/2}$  level of Er<sup>3+</sup> is populated through ET<sub>1</sub> process from the ground state  ${}^4\text{I}_{15/2}$ . The electrons located at  ${}^4\text{I}_{11/2}$  level of Er<sup>3+</sup> ions are further excited to  ${}^4\text{F}_{7/2}$  level *via* ET<sub>2</sub> process to accomplish population. With the help in NR relaxation involving in lattice phonons, the electrons at  ${}^4\text{F}_{7/2}$  level undergo NR transition to populate the  ${}^2\text{H}_{11/2}$ ,  ${}^4\text{S}_{3/2}$  and  ${}^4\text{F}_{7/2}$  levels of Er<sup>3+</sup> ions. The relatively weaker 537 nm and 560 nm green emissions are produced by the radiative transition (RT) from  ${}^2\text{H}_{11/2}$  and  ${}^4\text{S}_{3/2}$  level to the ground state  ${}^4\text{I}_{15/2}$  of Er<sup>3+</sup>, respectively. It is

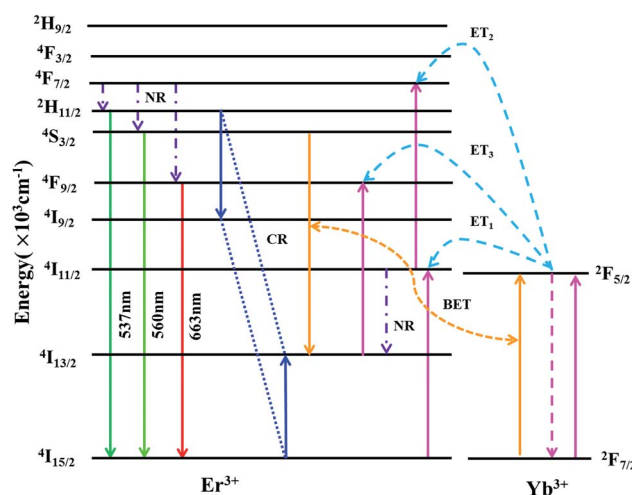


Fig. 11 Partial energy level diagram of Er<sup>3+</sup>/Yb<sup>3+</sup> and energy-transfer processes involved in the upconversion luminescence of F<sup>-</sup> co-doped EYBLO phosphor under 980 nm excitation.

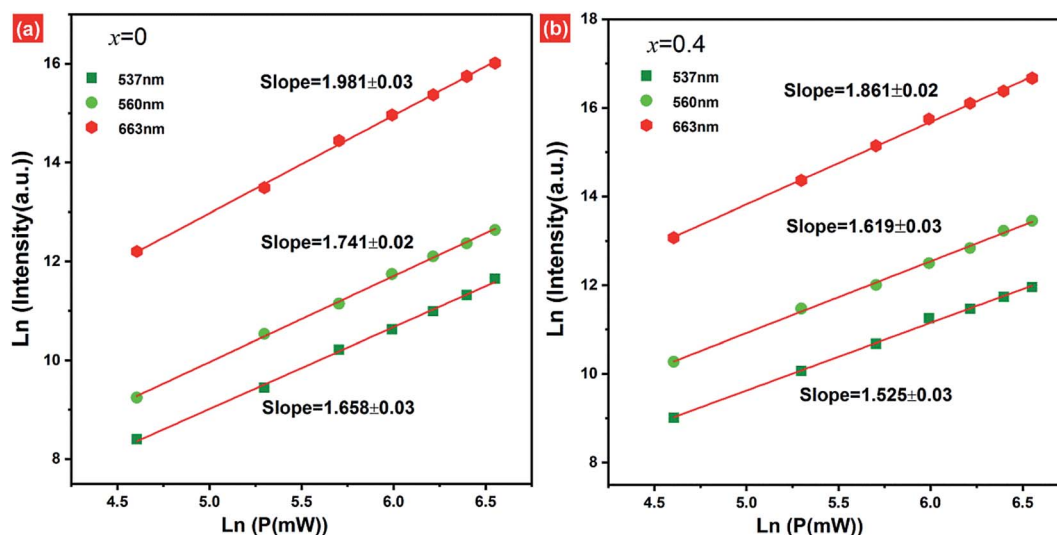
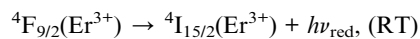
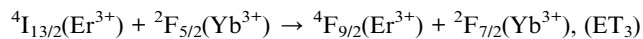
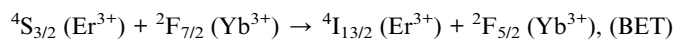
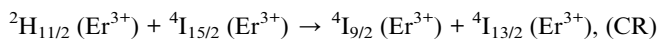
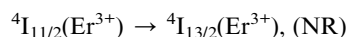
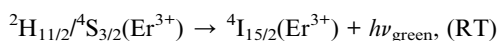
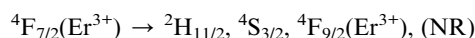
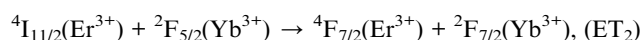
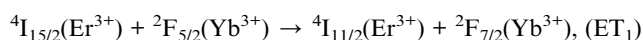


Fig. 10 Pump-power dependence of the upconversion emission intensity of EYBLO:xF<sup>-</sup> samples with (a)  $x = 0$  and (b)  $x = 0.4$  at 537 nm ( ${}^2\text{H}_{11/2} \rightarrow {}^4\text{I}_{15/2}$ ), 560 nm ( ${}^4\text{S}_{3/2} \rightarrow {}^4\text{I}_{15/2}$ ) and 663 nm ( ${}^4\text{F}_{9/2} \rightarrow {}^4\text{I}_{15/2}$ ) emission under 980 nm LD excitation.



obvious that the green emission UC luminescence is a two-phonon process, which is in good accordance with the slope value in Fig. 10. In the case of red emission, the NR transition from  $^4F_{7/2}$  level is not the only way to populate the  $^4F_{9/2}$  level of  $\text{Er}^{3+}$ . There exists another pathway of  $\text{ET}_3$  process to realize population of  $^4F_{9/2}$  level due to the UC red emission intensity increases more quickly than the green one when introduced  $\text{F}^-$  ions into EYBLO sample. The electrons at the  $^4I_{11/2}$  level of  $\text{Er}^{3+}$  also can populate  $^4I_{13/2}$  level through NR transition. In addition,  $\text{F}^-$  doping can lead to the contraction of crystal lattice and hence accelerates the CR process between  $\text{Er}^{3+}$  ions and BET process from  $\text{Er}^{3+}$  to  $\text{Yb}^{3+}$  ions, increasing the population of the  $^4I_{13/2}$  level which eventually leads to enhance the  $\text{ET}_3$  process to accomplish population of  $^4F_{9/2}$  level. The following expression can be used to give the brief description of the above the UC luminescence processes involved in green and red emissions:



### 3.4 Temperature sensing behavior

As mentioned above, in the case of  $\text{Er}^{3+}$  ions, UC emission bands centered at 537 nm and 560 nm are ascribed to the  $^2H_{11/2} \rightarrow ^4I_{15/2}$  and  $^4S_{3/2} \rightarrow ^4I_{15/2}$  transitions. Because of the small energy gap ( $700\text{--}800\text{ cm}^{-1}$ ) between the  $^2H_{11/2}$  and  $^4S_{3/2}$  levels of  $\text{Er}^{3+}$ , the state of  $^2H_{11/2}$  may also be populated from  $^4S_{3/2}$  by thermal excitation and a quasi-thermal equilibrium occurs between the two coupled levels.<sup>25,53</sup> In our as-prepared  $\text{F}^-$  doped EYBLO samples, it is interesting to observe that the UC emission intensity ratio of the emission bands centered at 537 nm to 560 nm could change with the variable of external temperature. Therefore, it could be used as optical temperature sensor for the present UC phosphor material (EYBLO: $\text{F}^-$ ). To investigate the temperature sensing behavior of as-synthesized phosphor, the FIR technique was employed. The green UC emission spectra of EYBLO:0.4 $\text{F}^-$  sample under various temperatures from 293 to 573 K at an excitation power density of near  $3\text{ W cm}^{-2}$  are shown in Fig. 12(a). In the present case, the low exciting power was utilized to reduce the heating effect caused by the excitation pumping source, and the emission spectra are normalized to the most intense emission peak at 560 nm. It is observed that

the peak positions of the two UC emission bands of  $^2H_{11/2} \rightarrow ^4I_{15/2}$  and  $^4S_{3/2} \rightarrow ^4I_{15/2}$  barely change varied with temperature, whereas the FIR of the two emission bands obviously increase with the rise of temperature. According to the Boltzmann distribution, with thermalization of populations at two thermally coupled levels  $^2H_{11/2}$  and  $^4S_{3/2}$  of  $\text{Er}^{3+}$ , the FIR of 537 nm and 560 nm green emission can be expressed as follow:<sup>54,55</sup>

$$\text{FIR} = \frac{I_{537}}{I_{560}} = \frac{N_H}{N_S} = \frac{g_H \omega_H \delta_H}{g_S \omega_S \delta_S} \exp\left(\frac{-\Delta E}{kT}\right) = B \exp\left(\frac{-\Delta E}{kT}\right) \quad (4)$$

where  $I_{537}$  and  $I_{560}$  are the integrated intensities of  $^2H_{11/2} \rightarrow ^4I_{15/2}$  (integrated from 500 to 542 nm) and  $^4S_{3/2} \rightarrow ^4I_{15/2}$  (integrated from 542 to 580 nm) transitions, respectively.  $N$ ,  $g$ ,  $\omega$ ,  $\delta$  are the number of ions, the degeneracy factors, the angular frequency, the emission cross-section of fluorescence transitions from the  $^2H_{11/2}$  and  $^4S_{3/2}$  levels to  $^4I_{15/2}$  level, respectively.  $\Delta E$  is the energy gap between the  $^2H_{11/2}$  and  $^4S_{3/2}$  levels,  $k$  is the Boltzmann constant,  $T$  is the absolute temperature, and the pre-exponential constant is given by  $B = g_H \omega_H \delta_H / g_S \omega_S \delta_S$ .

The monolog plot of the FIR of UC green emissions at 537 nm and 560 nm as a function of inverse absolute temperature in the range of 293–573 K is shown in Fig. 12(b). The linear dependence of the curve demonstrates the suitability of the phosphor in temperature sensing application. The experimental data could be fitted by a straight line with a slope of about 1157.04 and an intercept of about 2.25, respectively. The dependence of FIR of two green UC emissions on the absolute temperature is shown in Fig. 12(c). The FIR increases from 0.20 to 1.25 with increasing the temperature from 293 K to 573 K. The pre-exponential constant  $B$  value obtained using the above expression, is found to be near 9.48 according to the best curve fitting for the experiment data. As a consequence, the energy gap  $\Delta E$  is evaluated to be about  $801\text{ cm}^{-1}$ . This slightly deviation of  $\Delta E$  value from the actual value ( $700\text{--}800\text{ cm}^{-1}$ ) may be due to the fluctuations of the laser power and the absorption of the fluorescence by the host matrix during the recording of the spectra.<sup>48</sup> In addition, for the practical application of an optical temperature sensor, the relative sensor sensitivity ( $S$ ) is a very important reference parameter, which has been calculated using the following formula:<sup>54</sup>

$$S = \frac{d\text{FIR}}{dT} = \text{FIR} \left( \frac{-\Delta E}{kT^2} \right) = B \left( \frac{-\Delta E}{kT^2} \right) \exp\left(\frac{-\Delta E}{kT}\right) \quad (5)$$

The calculated values of sensitivity  $S$  as a function of the absolute temperature are plotted in Fig. 12(d). At the temperature of 523 K, the sensitivity of  $\text{F}^-$  doped EYBLO reaches its maximal value of about  $44.57 \times 10^{-4}\text{ K}^{-1}$ . Moreover, for the  $\text{F}^-$ -free doped EYBLO sample, similar study about temperature sensing behavior was conducted (ESI, Fig. S6<sup>†</sup>). It can be seen that the sensitivity keeps increasing in our experimental temperature range, and the maximal value of about  $42.26 \times 10^{-4}\text{ K}^{-1}$  is realized at the temperature of 523 K, which is lower than that of  $\text{F}^-$  doped sample. The results indicate that the sensor sensitivity could be improved by incorporation of  $\text{F}^-$  ions into the host lattice. It is worthwhile to compare the sensitivity results with the other  $\text{Er}^{3+}\text{--Yb}^{3+}$  co-doped oxide UC materials for





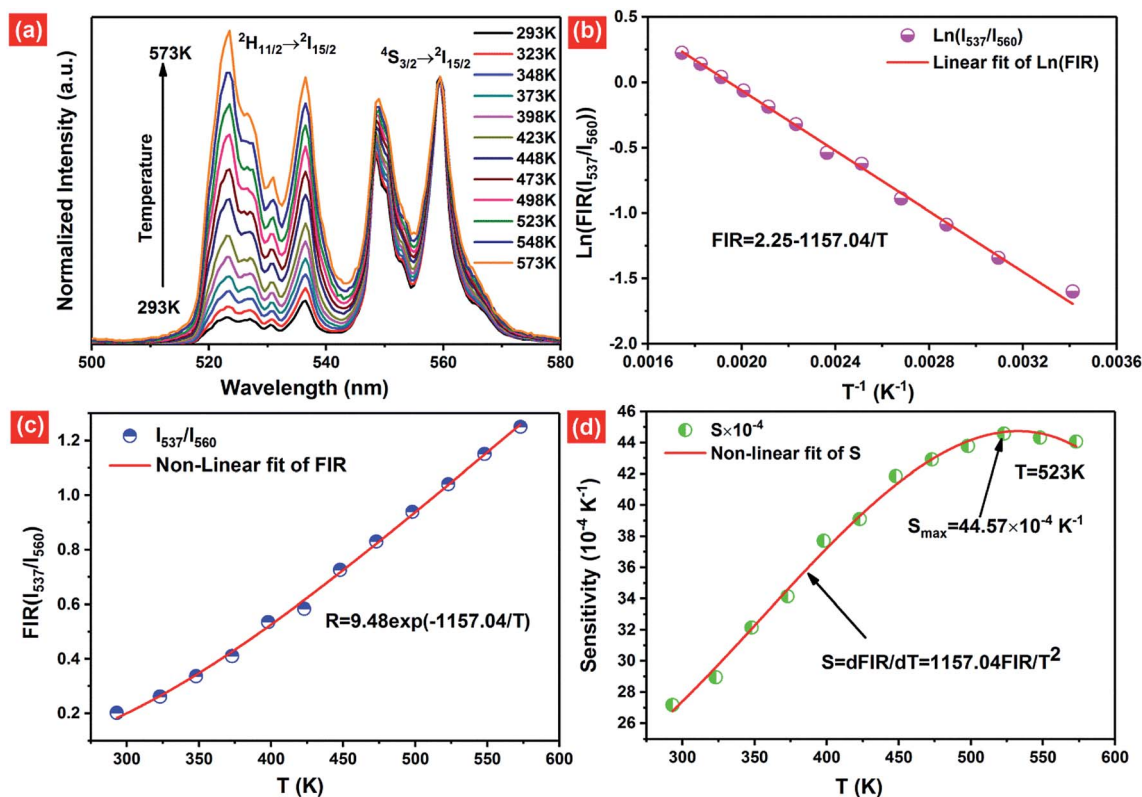


Fig. 12 (a) Temperature dependence of the green UC luminescence spectra within the range from 500 nm to 580 nm of EYBLO:0.4F<sup>-</sup> samples under 980 nm excitation (the spectra are normalized to the emission peak at 560 nm). The excitation power density is 3 W cm<sup>-2</sup>. Upconversion-based temperature-sensing behavior of EYBLO:0.4F<sup>-</sup> samples: (b) monolog plot of the FIR as a function of the inverse absolute temperature; (c) FIR relative to the temperature; (d) sensor sensitivity as a function of temperature.

temperature sensing (ESI, Table S1†). Compare with other oxide UC materials, the temperature sensitivity of EYBLO:F<sup>-</sup> is located at a moderate level, but it remains stable at higher temperature ranges. The results demonstrate that Ba<sub>3</sub>Lu<sub>4</sub>O<sub>9</sub> is a good host matrix for UC based phosphor, and F<sup>-</sup> doped EYBLO phosphor can be used in display device and as an excellent temperature sensor with high sensitivity and wide temperature ranges. In addition, this research may be extended to provide a practical method to enhance UC luminescence and temperature sensitivity in other high-quality optical temperature-sensing material by incorporation of F<sup>-</sup> ions.

## 4. Conclusions

In summary, F<sup>-</sup> ions co-doped Ba<sub>3</sub>Lu<sub>4</sub>O<sub>9</sub>:Er<sup>3+</sup>/Yb<sup>3+</sup> phosphors were synthesized by a solid-state reaction method. By doping appropriate F<sup>-</sup> ions into the lattices, the content of higher phonon energy impurities (OH<sup>-</sup> and CO<sub>2</sub>) could be reduced and the sample crystallinity could be improved. The F<sup>-</sup> doping concentration and sintering temperature are optimized to be  $x = 0.4$  and  $T = 1500$  °C to get highest luminescence yield. The upconversion mechanism to produce green and red luminescence remains unchanged after incorporation of F<sup>-</sup> ions, and the involved upconversion process occurs comparatively easily to saturate in F<sup>-</sup> co-doped sample than the F<sup>-</sup>-free samples. Under 980 nm laser diode excitation, the EYBLO:0.4F<sup>-</sup> sample

shows nearly 5- and 7.5-fold enhancements of green and red emissions compared with F<sup>-</sup>-free doped EYBLO, respectively. The enhancements of emission intensities are attributed to the fact that the substitution of O<sup>2-</sup> with F<sup>-</sup> can modify the local crystal field environment of Er<sup>3+</sup> ions and lower its site symmetry, leading to break the 4f–4f forbidden transitions to enhance the UC luminescence. The red/green emission intensity ratios keep increasing monotonically with the F<sup>-</sup> contents due to that F<sup>-</sup> doping can lead to the contraction of crystal lattice and hence accelerate the CR (<sup>2</sup>H<sub>11/2</sub> (Er<sup>3+</sup>) + <sup>4</sup>I<sub>15/2</sub> (Er<sup>3+</sup>) → <sup>4</sup>I<sub>9/2</sub> (Er<sup>3+</sup>) + <sup>4</sup>I<sub>13/2</sub> (Er<sup>3+</sup>)) process between Er<sup>3+</sup> ions and BET (<sup>4</sup>S<sub>3/2</sub> (Er<sup>3+</sup>) + <sup>2</sup>F<sub>7/2</sub> (Yb<sup>3+</sup>) → <sup>4</sup>I<sub>13/2</sub> (Er<sup>3+</sup>) + <sup>2</sup>F<sub>5/2</sub> (Yb<sup>3+</sup>)) process from Er<sup>3+</sup> to Yb<sup>3+</sup> ions, increasing the population of the <sup>4</sup>I<sub>13/2</sub> level which eventually leads to populate the <sup>4</sup>F<sub>9/2</sub> level. Meanwhile, the temperature sensing properties could be enhanced by incorporation of F<sup>-</sup> ions, and the maximum sensitivity is found to be  $44.57 \times 10^{-4} \text{ K}^{-1}$  at 523 K. The results indicate that F<sup>-</sup> doped EYBLO phosphor can be used in display device as a temperature sensor with high sensitivity and wide temperature ranges.

## Acknowledgements

This project supported by the Natural Science Foundation of China (51304086, 11464017), the Natural Science Foundation of Jiangxi Province (20132BAB206020), the Science and



Technology Research Plan of Jiangxi Education Department (GJJ14408), the Science and Technology Landing Plan for Colleges of Jiangxi Province (KJLD14045), Foundation of Science and Technology Pillar Program in Industrial Field of Jiangxi Province (20123BBE50075), Natural Science Funds for Distinguished Young Scholar of Jiangxi Province and the Program of Qingjiang Excellent Young Talents of Jiangxi University of Science and Technology.

## References

- 1 F. Auzel, *Chem. Rev.*, 2004, **104**, 139–173.
- 2 F. Wang, R. Deng, J. Wang, Q. Wang, Y. Han, H. Zhu, X. Chen and X. Liu, *Nat. Mater.*, 2011, **10**, 968–973.
- 3 X. Li, F. Zhang and D. Zhao, *Chem. Soc. Rev.*, 2015, **44**, 1346–1378.
- 4 M. Liu, M. Gu, Y. Tian, P. Huang, L. Wang, Q. Shi and C. Cui, *J. Mater. Chem. C*, 2017, **5**, 4025–4033.
- 5 S. Liu, X. Ye, S. Liu, M. Chen, H. Niu, D. Hou and W. You, *J. Am. Ceram. Soc.*, 2017, DOI: 10.1111/jace.14888.
- 6 H. Dong, L. Sun and C. Yan, *Chem. Soc. Rev.*, 2015, **44**, 1608–1634.
- 7 F. Wang and X. Liu, *Chem. Soc. Rev.*, 2009, **38**, 976–989.
- 8 W. Niu, S. Wu, S. Zhang and L. Li, *Chem. Commun.*, 2010, **46**, 3908–3910.
- 9 F. Wang, Y. Han, C. S. Lim, Y. Lu, J. Wang, J. Xu, H. Chen, C. Zhang, M. Hong and X. Liu, *Nature*, 2010, **463**, 1061–1065.
- 10 A. S. Oliveira, M. T. de Araujo, A. S. Gouveia-Neto, A. S. B. Sombra, J. A. Medeiros Neto and N. Aranha, *J. Appl. Phys.*, 1998, **83**, 604–606.
- 11 D. Li, W. Qin, T. Aidilibike, P. Zhang, S. Liu, L. Wang and S. Li, *J. Alloys Compd.*, 2016, **675**, 31–36.
- 12 Y. Bai, Y. Wang, K. Yang, X. Zhang, G. Peng and Y. Song, *J. Phys. Chem. C*, 2008, **112**, 12259–12263.
- 13 S. Liu, M. Chen, S. Liu, H. Niu, X. Ye, D. Hou and W. You, *Acta Opt. Sin.*, 2017, **37**, 0616002.
- 14 H. Guo, Z. Li, H. Qian, Y. Hu and I. N. Muhammad, *Nanotechnology*, 2010, **21**, 125602.
- 15 D. Li, B. Dong, X. Bai, Y. Wang and H. Song, *J. Phys. Chem. C*, 2010, **114**, 8219–8226.
- 16 Q. Cheng, J. Sui and W. Cai, *Nanoscale*, 2012, **4**, 779–784.
- 17 X. Chen, W. Zhang and Q. Zhang, *Phys. B*, 2011, **406**, 1248–1252.
- 18 R. Yan and Y. Li, *Adv. Funct. Mater.*, 2005, **15**, 763–770.
- 19 Y. Huang, K. Jang, X. Wang and C. Jiang, *J. Rare Earths*, 2008, **26**, 490–494.
- 20 Z. Zhao, Y. Xu, M. Ji and H. Zhang, *Electrochim. Acta*, 2013, **109**, 645–650.
- 21 J. Wang, X. Jing, C. Yan, J. Lin and F. Liao, *J. Lumin.*, 2006, **121**, 57–61.
- 22 X. Ye, Y. Luo, S. Liu, D. Hou, W. You and L. Xia, *Chin. J. Lumin.*, 2016, **37**, 1203–1212.
- 23 R. Sun, K. Chen, X. Wu, D. Zhao and Z. Sun, *CrystEngComm*, 2013, **15**, 3442–3447.
- 24 A. Li, D. Xu, H. Lin, L. Yao, S. Yang, Y. Shao, Y. Zhang and Z. Chen, *Phys. Chem. Chem. Phys.*, 2017, **19**, 15693–15700.
- 25 L. Li, C. Guo, S. Jiang, D. K. Agrawal and T. Li, *RSC Adv.*, 2014, **4**, 6391–6396.
- 26 B. P. Singh, A. K. Parchur, R. S. Ningthoujam, P. V. Ramakrishna, S. Singh, P. Singh, S. B. Rai and R. Maalej, *Phys. Chem. Chem. Phys.*, 2014, **16**, 22665–22676.
- 27 X. Wang, X. Kong, Y. Yu, Y. Sun and H. Zhang, *J. Phys. Chem. C*, 2007, **111**, 15119–15124.
- 28 Y. Tian, B. Tian, C. Cui, P. Huang, L. Wang and B. Chen, *RSC Adv.*, 2015, **5**, 14123–14128.
- 29 J. Liao, L. Nie, Q. Wang, S. Liu, H. Wen and J. Wu, *RSC Adv.*, 2016, **6**, 35152–35159.
- 30 X. Ye, Y. Luo, S. Liu, D. Hou and W. You, *J. Alloys Compd.*, 2017, **701**, 806–815.
- 31 J. Krüger and H. Müller-Buschbaum, *Z. Anorg. Allg. Chem.*, 1984, **512**, 59–64.
- 32 M. Thirumoorthi and J. T. J. Prakash, *Superlattices Microstruct.*, 2016, **89**, 378–389.
- 33 X. Jia, Y. Zhou, J. Zheng, Y. Li, H. Zou and R. Xie, *J. Alloys Compd.*, 2016, **688**, 679–684.
- 34 Y. V. Yermolayeva, A. V. Tolmachev, M. V. Dobrotvorskaya and O. M. Vovk, *J. Alloys Compd.*, 2011, **509**, 5320–5325.
- 35 J. Yu, Y. Yang, R. Fan, D. Liu, L. Wei, S. Chen, L. Li, B. Yang and W. Cao, *Inorg. Chem.*, 2014, **53**, 8045–8053.
- 36 J. Yu, J. Yu, W. Ho, Z. Jiang and L. Zhang, *Chem. Mater.*, 2002, **14**, 3808–3816.
- 37 H. Lu, X. Yu, S. Yang, H. Yang and S. Tu, *Fuel*, 2016, **165**, 215–223.
- 38 S. Saha, S. Das, U. K. Ghorai, N. Mazumder, B. K. Gupta and K. K. Chattopadhyay, *Dalton Trans.*, 2013, **42**, 12965–12974.
- 39 Y. Bai, Y. Wang, G. Peng, K. Yang, X. Zhang and Y. Song, *J. Alloys Compd.*, 2009, **478**, 676–678.
- 40 K. Mishra, S. K. Singh, A. K. Singh and S. B. Rai, *Mater. Res. Bull.*, 2013, **48**, 4307–4313.
- 41 Z. Chen, T. Chen, W. Gong, W. Xu, D. Wang, Q. Wang and A. Srivastava, *J. Am. Ceram. Soc.*, 2013, **96**, 1857–1862.
- 42 Y. Gao, M. Fan, Q. Fang and F. Yang, *New J. Chem.*, 2014, **38**, 146–154.
- 43 Q. Cheng, J. Sui and W. Cai, *Nanoscale*, 2012, **4**, 779–784.
- 44 S. H. Lee, H. Y. Koo, D. S. Jung, J. Han and Y. Kang, *Opt. Mater.*, 2009, **31**, 870–875.
- 45 P. Dai, X. Zhang, P. Sun, J. Yang, L. Wang, S. Yan and Y. Liu, *J. Am. Ceram. Soc.*, 2012, **95**, 1447–1453.
- 46 W. Yin, L. Zhao, L. Zhou, Z. Gu, X. Liu, G. Tian, S. Jin, L. Yan, W. Ren, G. Xing and Y. Zhao, *Chem.–Eur. J.*, 2012, **18**, 9239–9245.
- 47 D. Xu, C. Liu, J. Yan, S. Yang and Y. Zhang, *J. Phys. Chem. C*, 2015, **119**, 6852–6860.
- 48 D. Xu, H. Lin, A. Li, S. Yang and Y. Zhang, *J. Mater. Chem. C*, 2015, **3**, 9869–9876.
- 49 M. K. Mahata, T. Koppe, T. Mondal, C. Brusewitz, K. Kumar, V. Kumar Rai, H. Hofsass and U. Vetter, *Phys. Chem. Chem. Phys.*, 2015, **17**, 20741–20753.
- 50 A. Li, D. Xu, Y. Zhang, H. Lin, S. Yang, Z. Chen and Y. Shao, *J. Am. Ceram. Soc.*, 2016, **99**, 1657–1663.
- 51 P. Li, Z. Wang, Z. Yang and Q. Guo, *J. Mater. Chem. C*, 2014, **2**, 7823–7829.



- 52 D. R. G. M. Pollnau, S. R. Lüthi and H. U. Güdel, *Phys. Rev. B: Condens. Matter Mater. Phys.*, 2000, **61**, 3337–3346.
- 53 Y. Tian, Y. Tian, P. Huang, L. Wang, Q. Shi and C. Cui, *Chem. Eng. J.*, 2016, **297**, 26–34.
- 54 C. D. S. Brites, P. P. Lima, N. J. O. Silva, A. Millán, V. S. Amaral, F. Palacio and L. D. Carlos, *New J. Chem.*, 2011, **35**, 1177–1183.
- 55 B. Dong, B. Cao, Y. He, Z. Liu, Z. Li and Z. Feng, *Adv. Mater.*, 2012, **24**, 1987–1993.

